

# DERIVATION OF THIN PLATE BENDING ELEMENTS WITH ONE DEGREE OF FREEDOM PER NODE: A SIMPLE THREE NODE TRIANGLE

E. OÑATE AND M. CERVERA

*E.T.S. Ingenieros de Caminos, Canales y Puertos, Universidad Politécnica de Catalunya, Gran Capitán s/n,  
08034 Barcelona, Spain*

## ABSTRACT

A general methodology for deriving thin plate bending elements with a single degree of freedom per node is presented. The formulation is based on the combination of a standard  $C_0$  finite element interpolation for the deflection field with an independent approximation of the curvatures which are expressed in terms of the deflection gradient along the sides using a finite volume-like approach. The formulation is particularized for the simplest element of the family, i.e. the three node triangle with three degrees of freedom. The potential of the new element is shown through different examples of application.

KEY WORDS Thin plate bending elements Finite volume method Finite element method

## INTRODUCTION

This paper deals with the development of thin plate bending finite elements using only out-of-plane translational nodal degrees of freedom. Indeed, these elements could be very advantageous over more traditional and complex plate elements, especially in the field of large size non-linear problems in statics and dynamics.

The idea of using the deflection as the only variable for plate bending analysis is not new and most finite difference (FD) procedures are based on this approach<sup>1,11</sup>. The obvious difficulties of FD techniques are the treatment of boundary conditions and the problems for dealing with non-orthogonal or unstructured grids.

Several authors have tried to derive finite elements with the lateral deflection as the only nodal variable. So far the methods proposed limit their applicability to triangular element shapes only. Barnes<sup>2</sup> proposed a method for deriving a three node triangle with 3 nodal degrees of freedom (DOF) based on the computation of the curvatures in terms of the normal rotations at the mid-side points determined from the nodal deflections of adjacent elements. This method has also been exploited by Hampshire *et al.*<sup>3</sup> assuming that the elements are hinged together at their common boundaries, the bending stiffness being represented by torsional springs resisting the rotations about the hinge lines. These ideas have recently been extended by Brunet and Sabourin<sup>19</sup> to derive 3 node plate and shell triangles involving translational DOF only for sheet-forming analysis. Phaal and Calladine<sup>4,5</sup> have proposed a similar class of triangles for plate and flat shell analysis. The derivation of these elements is based on the concept of 'overlapping hinged bending elements'. The basic idea is to represent the deflection field using a complete quadratic polynomial defined over the six nodes patch formed by three

elements which can thus be considered as a six node macro-element. This procedure requires a careful identification of the element patches, and it involves the inversion of a  $3 \times 3$  matrix for each patch. Also, fictitious external nodes are needed to impose the boundary conditions at the plate edges.

In this paper an alternative methodology for deriving thin plate bending elements with a single degree of freedom per node is presented. The formulation is based on the interpolation of the deflection field inside each element using a  $C_0$  approximation. An independent assumed curvature field is then chosen and this is related to the deflection gradient (i.e. the rotations) along the sides using a finite volume-like approach. Finally, the deflection gradient along the sides is computed in terms of the nodal deflections of adjacent elements in a straight-forward manner.

The formulation proposed is completely general and it allows to derive thin plate bending elements with a single degree of freedom per node of triangular and quadrilateral shapes with different approximations. For the sake of conciseness only the simplest element of the family, i.e. the three node triangle with three degrees of freedom will be derived and assessed in detail here.

The layout of the paper is the following. In the next section the basic ideas of the formulation proposed are presented in their general form. Then the formulation is particularized to the development of a simple three node triangular element with only three nodal degrees of freedom. Details of the derivation of the element stiffness matrix and the load vector, the imposition of boundary conditions and the evaluation of stress resultants are also given. Finally, the efficiency of the new element is checked with some examples of application.

### BASIC THEORY

Let us consider a plate with the sign criterion for the vertical deflection  $w$  and the rotations  $\theta_x$ ,  $\theta_y$ , as shown in *Figure 1*. We will assume Kirchhoff's orthogonality conditions for thin plate analysis to hold, i.e.,

$$\theta_x = \frac{\partial w}{\partial x} \quad \text{and} \quad \theta_y = \frac{\partial w}{\partial y} \quad (1)$$

Under these conditions the curvature field can be expressed as<sup>11</sup>:

$$\kappa = [\kappa_x, \kappa_y, \kappa_{xy}]^T = \left[ -\frac{\partial^2 w}{\partial x^2}, -\frac{\partial^2 w}{\partial y^2}, -2 \frac{\partial^2 w}{\partial x \partial y} \right]^T = \mathbf{L}w \quad (2a)$$

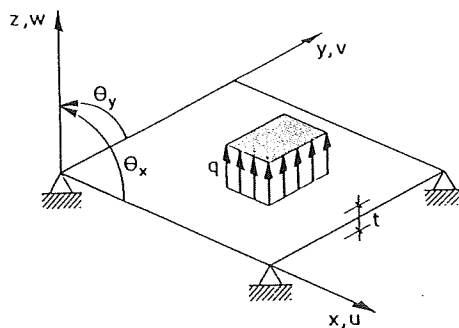


*Figure 1* Sign convention for the deflection and the rotations in a plate

with the differential operator  $\mathbf{L}$  defined as:

$$\mathbf{L} = \left[ -\frac{\partial^2}{\partial x^2}, -\frac{\partial^2}{\partial y^2}, -2\frac{\partial^2}{\partial x\partial y} \right]^T \quad (2b)$$

The constitutive relationship between bending moments and curvatures can be written as:

$$\mathbf{m} = [M_x, M_y, M_{xy}]^T = \mathbf{D}\boldsymbol{\kappa} \quad (3)$$

with

$$\mathbf{D} = \frac{Et^3}{12(1-\nu^2)} \begin{bmatrix} 1 & \nu & 0 \\ \nu & 1 & 0 \\ 0 & 0 & \frac{1-\nu}{2} \end{bmatrix} \quad (4)$$

where  $E$  and  $\nu$  are the Young's modulus and the Poisson's ratio, respectively. The sign criterion for bending moments can be seen in *Figure 2*.

The principle of virtual work (PVW) is written in its simpler form as:

$$\iint_A \delta\boldsymbol{\kappa}^T \mathbf{m} \, dA = \iint_A \delta w q \, dA \quad (5)$$

where virtual curvatures  $\delta\boldsymbol{\kappa}$  and virtual deflections  $\delta w$  are related by  $\delta\boldsymbol{\kappa} = \mathbf{L}\delta w$ ,  $A$  is the area of the plate and  $q$  the intensity of an uniformly distributed vertical load.

*Mixed formulation*

The PVW can be rewritten substituting (3) into (5) to give:

$$\iint_A \delta\boldsymbol{\kappa}^T \mathbf{D}\boldsymbol{\kappa} \, dA = \iint_A \delta w q \, dA \quad (6)$$

Equation (2a) can be written in integral form using the method of weighted residuals to give:

$$\iint_A \mathbf{W}^T [\boldsymbol{\kappa} - \mathbf{L}w] \, dA = 0 \quad (7a)$$

where

$$\mathbf{W} = \begin{bmatrix} W_1 & 0 & 0 \\ 0 & W_2 & 0 \\ 0 & 0 & W_3 \end{bmatrix} \quad (7b)$$

with  $W_i$  being arbitrary weighting functions.

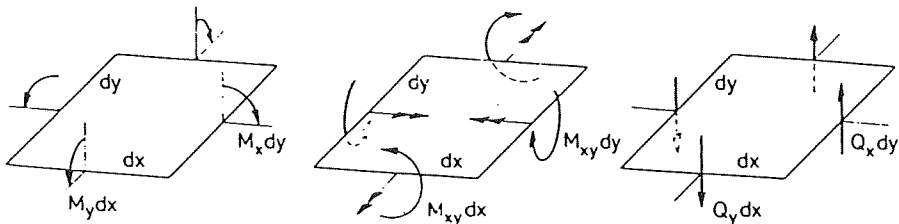


Figure 2 Sign criterion for bending moments and shear forces in a plate element

Equation (7) can be simplified by making:

$$W_i(\mathbf{x}) = \begin{cases} 1 & \mathbf{x} \in A_s \\ 0 & \mathbf{x} \notin A_s \end{cases} \quad (7c)$$

where  $A_s$  is an arbitrary subdomain of the plate, and then integrating by parts the term involving the deflection to give:

$$\iint_{A_s} \kappa \, dA = \int_{\Gamma_s} \mathbf{T} \nabla w \, d\Gamma \quad (8)$$

where

$$\mathbf{T} = \begin{bmatrix} n_x & 0 \\ 0 & n_y \\ n_y & n_x \end{bmatrix}, \quad \nabla = \begin{pmatrix} \frac{\partial}{\partial x} \\ \frac{\partial}{\partial y} \end{pmatrix} \quad (9)$$

and  $\Gamma_s$  is the boundary of the subdomain  $A_s$ .

Equations (6) and (8) are the basis for the finite element discretization presented in the next section.

**Remark 1.** The choice of  $W_i$  leading to (8) is typical of finite volume methods (FVM), extensively used in thermal and fluid flow problems<sup>6,7,10</sup>. For a recent discussion of the FVM in the context of structural mechanics see References 8 and 9.

**Remark 2.** Note that (8) is satisfied for any patch of area  $A_s$  surrounded by a boundary  $\Gamma_s$ .

**Remark 3.** Note also that (8) involves the computation of the deflection gradient along the boundary  $\Gamma_s$  of the subdomain considered. This poses some difficulties when a  $C_0$  finite element approximation is used for the deflection, as this leads to a discontinuous gradient of  $w$  across boundaries of adjacent elements. This problem can be overcome by computing the deflection gradient in an element boundary as the average of the gradients contributed by the two elements sharing the boundary. More details of this averaging procedure are given in the next section.

## FINITE ELEMENT DISCRETIZATION

The plate is discretized in a mesh of  $C_0$  finite elements in the standard form<sup>12,13</sup>. The deflection field is written in terms of the nodal deflections as:

$$w = \sum_{i=1}^n N_{w_i} \bar{w}_i = \mathbf{N}_w \bar{\mathbf{w}} \quad (10)$$

where  $\bar{w}_i$  are nodal deflection values,  $\bar{\mathbf{w}} = [\bar{w}_1, \dots, \bar{w}_n]^T$ ,  $N_{w_i}$  is the shape function of node  $i$  and  $n$  is the number of nodes in the mesh.

The three curvatures can now be interpolated over the mesh using a  $C_0$  continuous approximation as:

$$\kappa = \sum_{i=1}^p N_{\gamma_i} \mathbf{I}_3 \bar{\kappa}_i = \mathbf{N}_\gamma \bar{\kappa} \quad (11)$$

where  $p$  is the total number of interpolating points in the mesh;  $\bar{\kappa}_i$  are the curvature values at

the  $i$ th interpolating point;  $N_{\gamma_i}$  is the curvature interpolating function for point  $i$ ;  $\mathbf{I}_3$  is the  $3 \times 3$  unit matrix and

$$\mathbf{N}_\gamma = [N_{\gamma_1}\mathbf{I}_3, \dots, N_{\gamma_p}\mathbf{I}_3]; \quad \bar{\boldsymbol{\kappa}} = [\bar{\boldsymbol{\kappa}}_1^T, \dots, \bar{\boldsymbol{\kappa}}_p^T]^T \quad (12)$$

Substitution of (10) and (11) in (8) gives:

$$\left[ \iint_{A_i} \mathbf{N}_\gamma \, d\Omega \right] \bar{\boldsymbol{\kappa}} = \left[ \int_{\Gamma_i} \mathbf{T} \nabla N_{w_j} \right] \bar{\mathbf{w}} \quad i = 1, \dots, p \quad (13)$$

where  $A_i$  and  $\Gamma_i$  are respectively the area and the boundary corresponding to the 'domain' associated with the  $i$ th curvature interpolating point (see Remark 3).

Equation (13) can be written in matrix form as:

$$\mathbf{P} \bar{\boldsymbol{\kappa}} = \mathbf{H} \bar{\mathbf{w}} \quad (14)$$

where  $\mathbf{P}$  and  $\mathbf{H}$  are  $3p \times 3p$  and  $3p \times n$  matrices respectively, given by:

$$\mathbf{P}_{ij} = \iint_{A_i} N_{\gamma_j} \mathbf{I}_3 \, d\Omega \quad (15a)$$

$$\mathbf{H}_{ij} = \int_{\Gamma_i} \mathbf{T}(\nabla N_{w_j}) \, d\Gamma \quad (15b)$$

Equation (14) allows us to obtain the discrete curvature variables in terms of the nodal deflections as:

$$\bar{\boldsymbol{\kappa}} = \mathbf{P}^{-1} \mathbf{H} \bar{\mathbf{w}} \quad (16)$$

Substituting (16) into (11) yields:

$$\boldsymbol{\kappa} = \mathbf{B} \bar{\mathbf{w}} \quad (17)$$

where the 'strain matrix'  $\mathbf{B}$  is given by:

$$\mathbf{B} = \mathbf{N}_\gamma \mathbf{P}^{-1} \mathbf{H} \quad (18)$$

A similar procedure can be followed to obtain the relationship between virtual curvatures and virtual deflections as:

$$\delta \boldsymbol{\kappa} = \mathbf{B} \delta \bar{\mathbf{w}} \quad (19)$$

where  $\mathbf{B}$  coincides with that of (18).

Substituting (10), (17) and (19) into (6) allows us to derive the global matrix equilibrium equations for the plate in the standard form:

$$\mathbf{K} \bar{\mathbf{w}} = \mathbf{f} \quad (20)$$

where the stiffness matrix and the equivalent nodal force vector for the whole mesh are given by:

$$\mathbf{K} = \iint_A \mathbf{B}^T \mathbf{D} \mathbf{B} \, dA \quad (21a)$$

$$\mathbf{f} = \iint_A \mathbf{N}_w^T q \, dA \quad (21b)$$

**Remark 4.** There are multiple options to define the area  $A_i$  and the boundary  $\Gamma_i$  of the 'domain' associated to each curvature interpolating point, and here again the finite volume

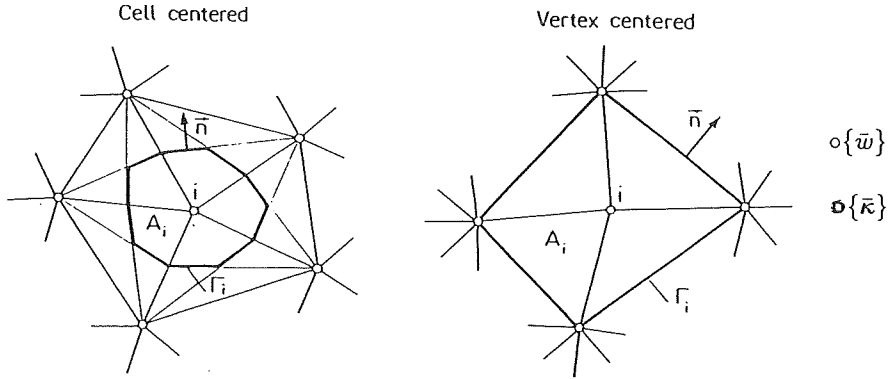


Figure 3 Cell centred and vertex centred domains surrounding a node  $i$

methodology can be used<sup>8,9</sup>. Figure 3 shows some alternatives based on the assumption that  $p = n$ , i.e., the curvature interpolating points coincide with the nodes and thus  $N_{\gamma_i} = N_{w_i}$ . Note that in the so-called ‘vertex centred’ approach the computation of the deflection gradients along interelemental sides requires the adequate averaging of the gradients contributed from the two element sharing the side, as mentioned in Remark 3. This aspect will be further detailed later.

**Remark 5.** The fields  $w$  and  $\kappa$  must satisfy certain compatibility conditions which ensure the existence of the solution for the mixed problem<sup>12</sup>. These conditions can be summarized as:

$$n_{\bar{\kappa}} \geq n_{\bar{w}} \tag{22}$$

where  $n_{\bar{\kappa}}$  and  $n_{\bar{w}}$  denote the number of available degrees of freedom for the curvature and deflection fields (after discounting the prescribed values). The proof of this condition can be seen in References 12 and 18.

### DISCONTINUOUS APPROXIMATION OF THE CURVATURES FIELD

The procedure presented above requires the inversion of the global matrix  $\mathbf{P}$  and this can be expensive for practical purposes. A way to overcome this difficulty is to define a discontinuous approximation of the curvatures field. Thus (11) can be written individually for each element as:

$$\kappa^{(e)} = \sum_{i=1}^{n_c} N_{\gamma_i}^{(e)} \mathbf{I}_3 \bar{\kappa}_i^{(e)} = \mathbf{N}_{\gamma}^{(e)} \bar{\kappa}^{(e)} \tag{23}$$

where  $n_c$  is the number of curvature interpolating points within element  $e$ ;  $N_{\gamma_i}^{(e)}$  are *discontinuous* shape functions and all other terms of (23) have the same meaning as in (11), but now they are referred to an individual element.

Equation (8) can now be particularized for an individual element to give:

$$\iint_{A_i^{(e)}} \kappa^{(e)} dA = \int_{\Gamma_i^{(e)}} \text{TV}w^{(e)} d\Gamma \tag{24}$$

where  $A_i^{(e)}$  and  $\Gamma_i^{(e)}$  are now the area and the boundary of the domain associated to the  $i$ th curvature interpolating point within the element. Some examples of typical ‘vertex-centred domains’ for piece-wise constant and linear discontinuous curvature interpolations in triangular and quadrilateral elements are shown in Figure 4.

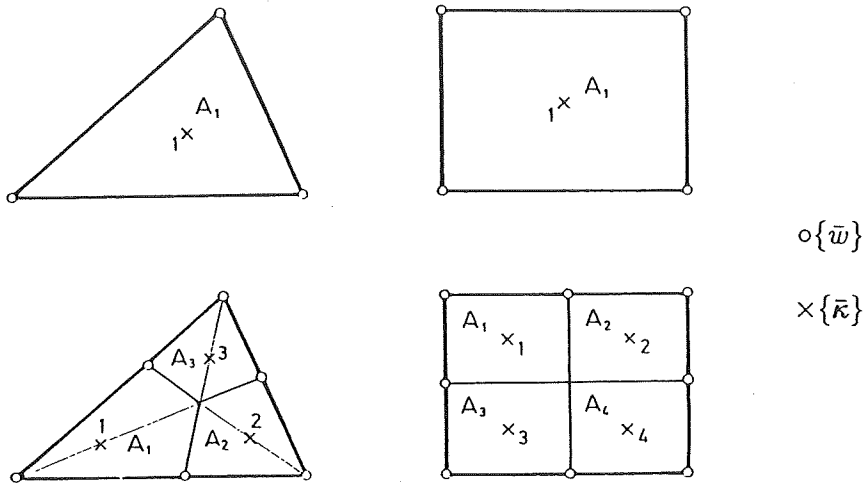


Figure 4 Typical vertex-centred domain for piece-wise constant and linear discontinuous curvatures interpolations over triangles and rectangles

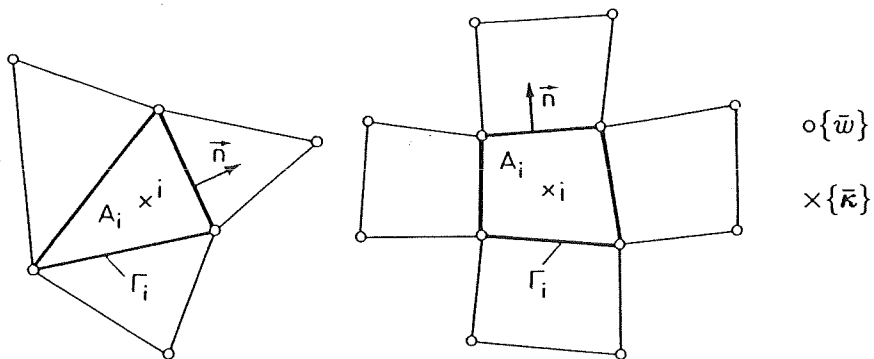


Figure 5 Typical patches associated to linear triangular and bilinear quadrilateral elements with a single curvature interpolating point (vertex-centred approach)

Equation (24) requires necessarily the computation of the deflection gradient along the element sides. This poses some difficulties due to the discontinuous nature of the term  $\nabla w$  between elements. As mentioned earlier, a simple method to overcome this problem is to compute the deflection gradient at a point of an element side as the average value of the gradients contributed to the point from the two elements sharing that particular side. Thus, the computation of the r.h.s. of (24) for each element involves necessarily the nodes included in the patch formed by this element and all adjacent elements. Figure 5 shows typical patches associated to linear triangular and bilinear quadrilateral elements with a single curvature interpolating point using a vertex centred type approach.

Substituting (10) and (23) into (24) allows us to relate the element curvature variables to the nodal deflections of the patch associated to each element as:

$$\mathbf{P}^{(e)} \bar{\mathbf{k}}^{(e)} = \mathbf{H}^{(e)} \mathbf{a}^{(e)} \tag{25}$$

where  $\mathbf{a}^{(e)} = [\bar{w}_1, \bar{w}_2, \dots, \bar{w}_{n_p}]^T$  and  $n_p$  is the number of nodes involved in the patch formed by element  $e$  and all adjacent elements sharing the sides of this element.

Matrices  $\mathbf{P}^{(e)}$  and  $\mathbf{H}^{(e)}$  are obtained as:

$$\mathbf{P}_{ij}^{(e)} = \iint_{A_i^{(e)}} N_{\gamma_j} \mathbf{I}_3 \, dA \quad i = 1, \dots, n_c; j = 1, \dots, n_c \quad (26)$$

$$H_{ij}^{(e)} = \int_{\Gamma_i^{(e)}} \mathbf{T}[\alpha \nabla N_{w_j}^{(e)} + \beta \nabla N_{w_j}^{(f)}] \, d\Gamma \quad i = 1, \dots, n_c; j = 1, \dots, n_p \quad (27)$$

where  $\alpha = 1$  and  $\beta = 0$  for the part of the domain boundary  $\Gamma_i^{(e)}$  located within the element, and  $\alpha = \beta = \frac{1}{2}$  for the part of  $\Gamma_i^{(e)}$  coinciding with the side shared by element  $e$  and an adjacent element  $f$ .

In (27)  $N_{w_j}^{(e)}$  denotes, as usual, the shape function of node  $j$  defined locally over element  $e$ .

**Remark 6.** Note that if a single curvature interpolating point at the element mid-point is used, the domain area and its boundary coincide with the element area and its boundary, respectively, i.e.  $A_i^{(e)} = A^{(e)}$  and  $\Gamma_i^{(e)} = \Gamma^{(e)}$  (see *Figures 3 and 4*).

**Remark 7.** The simple averaging procedure for estimation of the deflection derivative along the sides could be obviously improved by using more sophisticated derivative approximation procedures. Here the use of special smoothing techniques<sup>15</sup>, derivative recovery methods<sup>16</sup> or diffuse approximation<sup>17</sup> could prove to be advantageous and they should be explored.

The discontinuous nature of the curvatures field allows to eliminate the element curvature variables  $\tilde{\kappa}^{(e)}$  in terms of the nodal deflections of the patch from (25) as:

$$\tilde{\kappa}^{(e)} = [\mathbf{P}^{(e)}]^{-1} \mathbf{H}^{(e)} \mathbf{a}^{(e)} \quad (28)$$

The curvature matrix for the element is finally obtained substituting (28) into (23) to give:

$$\kappa^{(e)} = \mathbf{N}_{\gamma}^{(e)} [\mathbf{P}^{(e)}]^{-1} \mathbf{H}^{(e)} \mathbf{a}^{(e)} = \mathbf{B}^{(e)} \mathbf{a}^{(e)} \quad (29)$$

with

$$\mathbf{B}^{(e)} = \mathbf{N}_{\gamma}^{(e)} [\mathbf{P}^{(e)}]^{-1} \mathbf{H}^{(e)} \quad (30)$$

Substituting (30) into (6) yields the discretized equilibrium equations for the element in terms of the 'patch' nodal deflection variables  $\mathbf{a}^{(e)}$  in the standard form<sup>13</sup> as:

$$\mathbf{K}^{(e)} \mathbf{a}^{(e)} - \mathbf{f}^{(e)} = \mathbf{q}^{(e)} \quad (31)$$

where  $\mathbf{q}^{(e)}$  are the equilibrating nodal forces needed for global assembly purposes only and the stiffness matrix and the equivalent nodal force vector for the element are given by:

$$\mathbf{K}^{(e)} = \iint_{A^{(e)}} [\mathbf{B}^{(e)}]^T \mathbf{D} \mathbf{B}^{(e)} \, dA \quad (32)$$

$$\mathbf{f}^{(e)} = \iint_{A^{(e)}} [\mathbf{N}^{(e)T}, \mathbf{0}, \dots, \mathbf{0}]^T q \, dA \quad (33)$$

The columns of zeros in vector  $\mathbf{f}^{(e)}$  take into account the effect of the patch elements adjacent to element  $e$ , which obviously should not contribute to the nodal forces of this element.

The global equilibrium equations are obtained by assembly of the element contributions in the standard manner<sup>12,13</sup>.



**Remark 8.** Note that the equilibrium equation (31) for the element involve the nodal deflection variables of the patch formed by element  $e$  and all adjacent elements sharing the sides of that element. This naturally leads to a wider bandwidth in the global equations system after assembly than that arising from the standard finite element method.

The procedure presented is completely general and it allows us to derive plate bending elements with a single degree of freedom per node of quadrilateral and triangular shapes of any order. To clarify concepts the formulation will be particularized next to derive the simplest element of the family, i.e., the three node triangle with only 3 degrees of freedom, which shows a promising behaviour for plate analysis.

### DERIVATION OF A THREE NODE TRIANGULAR PLATE ELEMENT WITH 3 DOF

The geometry of the element is shown in *Figure 6*, where the patch of elements surrounding a particular element  $e$  with nodes  $i, j, k$  is shown.

The deflection field is linearly interpolated within each element using standard linear shape functions of the form:

$$N_i^{(e)} = \frac{1}{2A^{(e)}} (a_i^{(e)} + b_i^{(e)}x + c_i^{(e)}y) \tag{34a}$$

where

$$a_i^{(e)} = x_j y_k - x_k y_j, \quad b_i^{(e)} = y_j - y_k, \quad c_i^{(e)} = x_k - x_j \tag{34b}$$

and  $x_i, y_i$ , etc. are the coordinates of the element nodes. The superindex  $(e)$  is needed in  $a_i^{(e)}$ , etc. since node  $i$  can be shared by different elements.

The curvature field within each element is now expressed using a piece-wise constant approximation, i.e.  $N_{\gamma_i}^{(e)} = 1$  in (23), which naturally gives from (26):

$$\mathbf{P}^{(e)} = A^{(e)} \mathbf{I}_3 \tag{35}$$

As mentioned earlier, this curvature approximation corresponds to a vertex-centred approach in which the 'domain' surrounding each curvature interpolating point coincides with that of a single element.

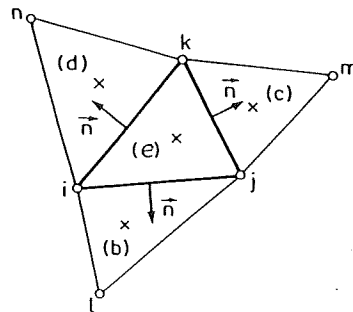


*Figure 6* Patch of three node triangles associated to a vertex-centred domain  $i, j, k$

The derivation of matrix  $\mathbf{H}^{(e)}$  follows the lines explained in the previous section. This involves a simple procedure if we first note that the external unit normal vector to a side  $ij$  of length  $l_{ij}$  (see *Figure 5*) is given by:

$$\mathbf{n} = \frac{1}{l_{ij}} [y_{ij}, -x_{ij}]^T \quad (36a)$$

with

$$y_{ij} = y_i - y_j, \quad x_{ij} = x_i - x_j \quad (36b)$$

The line integrals along the element sides of some characteristic terms of (27) are simply expressed in terms of 'patch' variables following the averaging procedure explained in the previous section. Thus, for side  $ij$  we have:

$$\int_{l_{ij}} n_x \frac{\partial w}{\partial x} d\Gamma = \frac{y_{ij}}{2} [(\bar{b}_i^{(e)} + \bar{b}_i^{(b)}), (\bar{b}_j^{(e)} + \bar{b}_j^{(b)}), \bar{b}_k^{(e)}, \bar{b}_l^{(b)}, 0, 0] \mathbf{a}^{(e)} \quad (37)$$

$$\int_{l_{ij}} n_y \frac{\partial w}{\partial y} d\Gamma = -\frac{x_{ij}}{2} [(\bar{c}_i^{(e)} + \bar{c}_i^{(b)}), (\bar{c}_j^{(e)} + \bar{c}_j^{(b)}), \bar{c}_k^{(e)}, \bar{c}_l^{(b)}, 0, 0] \mathbf{a}^{(e)} \quad (38)$$

where

$$\bar{b}_i^{(e)} = \frac{b_i^{(e)}}{2A^{(e)}}, \quad \bar{c}_i^{(e)} = \frac{c_i^{(e)}}{2A^{(e)}}, \quad \text{etc.} \quad (39)$$

and

$$\mathbf{a}^{(e)} = [w_i, w_j, w_k, w_l, w_m, w_n]^T \quad (40)$$

is the nodal deflections vector of the four elements patch corresponding to element  $e$ . A similar expression can be obtained for the integral  $\int_{l_{ij}} \left( n_y \frac{\partial w}{\partial x} + n_x \frac{\partial w}{\partial y} \right) d\Gamma$ . The derivation of matrix  $\mathbf{H}^{(e)}$  of (30) is straight-forward and its explicit form is given in *Table 1*.

The curvature matrix for the element is obtained using (30). The simple curvature approximation chosen for the element allows us to write:

$$\mathbf{B}^{(e)} = \frac{1}{A^{(e)}} \mathbf{H}^{(e)} \quad (41)$$

The stiffness matrix for the element is then simply obtained (for homogeneous material properties) as:

$$\mathbf{K}^{(e)} = \frac{1}{A^{(e)}} [\mathbf{H}^{(e)}]^T \mathbf{D} \mathbf{H}^{(e)} \quad (42)$$

*Table 1* Matrix  $\mathbf{H}^{(e)}$  for the 3 DOF basic plate triangle (BPT)

$$\mathbf{H}^{(e)} = \frac{1}{2} \begin{bmatrix} y_{ij}\bar{b}_i^{(b)} + y_{ki}\bar{b}_i^{(b)} & y_{ij}\bar{b}_j^{(e)} + y_{jk}\bar{b}_j^{(e)} & y_{jk}\bar{b}_k^{(e)} + y_{ki}\bar{b}_k^{(d)} & y_{ij}\bar{b}_l^{(b)} & y_{jk}\bar{b}_m^{(e)} & y_{ki}\bar{b}_n^{(d)} \\ -x_{ij}\bar{c}_i^{(b)} - x_{ki}\bar{c}_i^{(d)} & -x_{ij}\bar{c}_j^{(b)} - x_{jk}\bar{c}_j^{(e)} & -x_{jk}\bar{c}_k^{(e)} - x_{ki}\bar{c}_k^{(d)} & -x_{ij}\bar{c}_l^{(b)} & -x_{jk}\bar{c}_m^{(e)} & -x_{ki}\bar{c}_n^{(d)} \\ y_{ij}\bar{c}_i^{(b)} - x_{ij}\bar{b}_i^{(b)} + & y_{ij}\bar{c}_j^{(b)} - x_{ij}\bar{b}_j^{(b)} + & y_{jk}\bar{c}_k^{(e)} - x_{jk}\bar{b}_k^{(e)} + & y_{ij}\bar{c}_l^{(b)} - x_{ij}\bar{b}_l^{(b)} & y_{jk}\bar{c}_m^{(e)} - x_{jk}\bar{b}_m^{(e)} & y_{ki}\bar{c}_n^{(d)} - x_{ki}\bar{c}_n^{(d)} \\ + y_{ki}\bar{c}_i^{(d)} - x_{ki}\bar{b}_i^{(d)} & + y_{jk}\bar{c}_j^{(e)} - x_{jk}\bar{b}_j^{(e)} & + y_{ki}\bar{c}_k^{(d)} - x_{ki}\bar{c}_k^{(d)} & & & \end{bmatrix}$$

and the equivalent nodal force for a uniformly distributed load of intensity  $q$  is:

$$\mathbf{f}^{(e)} = \frac{qA^{(e)}}{3} [1, 1, 1, 0, 0, 0]^T \tag{43}$$

The global equilibrium equations are assembled in the standard manner from the element contributions, taking into account that the equation for an individual element relates the six nodal deflection variables of the corresponding four elements patch.

**Remark 9.** An alternative procedure for deriving matrix  $\mathbf{H}^{(e)}$  can be based in the definition of the deflection gradients along a side in terms of the *tangential* and *normal rotations* along that side. Since the tangential rotations are continuous along the side (i.e.  $\frac{\partial w}{\partial s} \Big|_{ij} = \frac{w_j - w_i}{l_{ij}}$ ) only the normal rotations need to be averaged using the values from the two adjacent elements. For shortness reasons the 3 DOF plate triangle above derived will be termed hereonwards BPT (for basic plate triangle) element.

### IMPOSITION OF THE BOUNDARY CONDITIONS

The practical application of the plate bending element described above requires the consideration of the various types of boundary conditions which are usual in plate bending analysis, that is, free edges, simply supported edges, clamped edges and fictitious symmetry edges.

A plate bending element which lies along a boundary belongs to a ‘patch’ where one of the contributing elements is missing (see *Figure 7*). For the purpose of derivation let us suppose that the element edge along the boundary is  $\Gamma_{ij}$ , and so, element  $b$  and node  $l$  are the ones missing in the corresponding patch. In this situation, a possible expression to compute the deflection gradient along the boundary side  $\Gamma_{ij}$  is:

$$\nabla w|_{\Gamma_{ij}} = \nabla w^{(e)}|_{\Gamma_{ij}} \tag{44}$$

In practice this implies making  $\alpha = 1$  and  $\beta = 0$  in (27) for the part of the line integral over  $\Gamma_i^{(e)}$  coinciding with  $\Gamma_{ij}$ .

**Remark 10.** This approximation can be obviously used if more than one side of the element lies along the boundary of the plate (corner nodes). The extension to these cases is straight-forward.

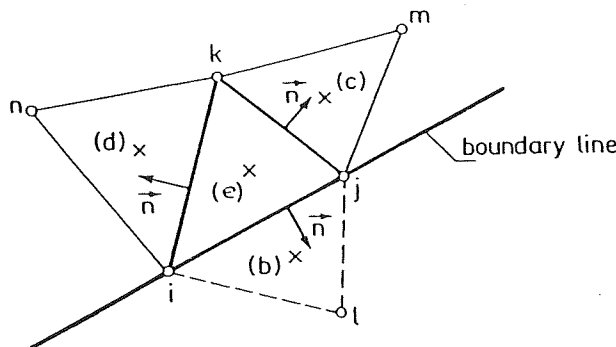


Figure 7 Triangular element lying along a boundary line

*Free and simply supported edges*

Consequently with the approximation in (44) the line integrals along the side  $\Gamma_{ij}$  of the terms appearing on the right hand side of (27) will be evaluated as:

$$\int_{\Gamma_{ij}} n_x \frac{\partial w}{\partial x} d\Gamma = y_{ij} [b_i^{(e)}, b_j^{(e)}, b_k^{(e)}, 0, 0, 0] \mathbf{a}^{(e)} \quad (45)$$

$$\int_{\Gamma_{ij}} n_y \frac{\partial w}{\partial y} d\Gamma = -x_{ij} [\bar{c}_i^{(e)}, \bar{c}_j^{(e)}, \bar{c}_k^{(e)}, 0, 0, 0] \mathbf{a}^{(e)} \quad (46)$$

instead of using the expressions (37) and (38).

The derivation of matrix  $\mathbf{H}^{(e)}$  for this case is again straight-forward and its explicit form can be found in Reference 18.

The conditions for a simply supported edge are simply obtained using this modified  $\mathbf{H}^{(e)}$  matrix and constraining the corresponding deflection degrees of freedom to a zero value. This can be done at the global equations solution level in the standard fashion<sup>12</sup>.

**Remark 11.** The conditions of zero bending moments and zero equivalent shear forces along a side (free edge) are natural in this formulation, as it derives from the PVW<sup>12,13</sup>.

*Fictitious symmetry edge*

If the fictitious symmetry edge lies along a line parallel to the global  $y$  axis the symmetry condition is simply:

$$\left. \frac{\partial w}{\partial x} \right|_{\Gamma_{ij}} = 0 \quad (47)$$

and the corresponding terms on the right hand side of (45) have to be zeroed. This is simply accomplished by setting  $b_i^{(e)} = b_j^{(e)} = b_k^{(e)} = 0$  in all the terms where these coefficients appear when evaluating the contribution of side  $\Gamma_{ij}$  to matrix  $\mathbf{H}^{(e)}$ . The corresponding  $\mathbf{H}^{(e)}$  matrix can be then easily evaluated and its explicit form can be found in Reference 18.

If the fictitious symmetry edge lies along a line parallel to the global  $x$  axis then the symmetry condition is:

$$\left. \frac{\partial w}{\partial y} \right|_{\Gamma_{ij}} = 0 \quad (48)$$

and this is enforced by making  $\bar{c}_i^{(e)} = \bar{c}_j^{(e)} = \bar{c}_k^{(e)} = 0$  in all the terms where these coefficients appear when evaluating the contribution of side  $\Gamma_{ij}$  to matrix  $\mathbf{H}^{(e)}$  (see for instance (46)).

*Clamped edge*

If the boundary edge is clamped the conditions that must be satisfied are:

$$w|_{\Gamma_{ij}} = 0 \quad (49)$$

$$\left. \frac{\partial w}{\partial n} \right|_{\Gamma_{ij}} = 0 \quad (50)$$

where  $n$  is the direction normal to the boundary  $\Gamma_{ij}$ . Condition (49) can be imposed at equation

solution level as in the simply supported case. If this condition holds, it is also true that:

$$\left. \frac{\partial w}{\partial s} \right|_{\Gamma_{ij}} = 0 \quad (51)$$

where  $s$  is the direction parallel to  $\Gamma_{ij}$ . Now, considering (50) and (51) together one can simply write:

$$\nabla w|_{\Gamma_{ij}} = \nabla w^{(e)}|_{\Gamma_{ij}} = \mathbf{0} \quad (52)$$

Then it is obvious that the corresponding  $\mathbf{H}^{(e)}$  matrix will be constructed as in (27), but disregarding the contribution from side  $\Gamma_{ij}$ . The explicit form of  $\mathbf{H}^{(e)}$  for this case can be found in Reference 18.

### EVALUATION OF STRESS RESULTANTS

The constant bending moment distribution within each single DOF triangle is obtained by the standard expression:

$$\mathbf{m}^{(e)} = \mathbf{DB}^{(e)}\mathbf{a}^{(e)} \quad (53)$$

where matrix  $\mathbf{B}^{(e)}$  is given by (30).

The computation of shear forces is not straight-forward. The relationship between shear forces and bending moments is given by:

$$\mathbf{q} = \begin{Bmatrix} Q_x \\ Q_y \end{Bmatrix} = \begin{bmatrix} \frac{\partial}{\partial x} & 0 & \frac{\partial}{\partial y} \\ 0 & \frac{\partial}{\partial y} & \frac{\partial}{\partial x} \end{bmatrix} \begin{Bmatrix} M_x \\ M_y \\ M_{xy} \end{Bmatrix} = \hat{\mathbf{L}}\mathbf{m} \quad (54)$$

The sign criterion for shear forces is shown in *Figure 2*.

A procedure to evaluate the shear forces is to smooth the discontinuous bending moment field and then to apply (54) to the resulting continuous field.

An alternative procedure is to use a similar methodology to that used to approximate the curvature field. Thus, integrating (54) over each element domain gives:

$$\iint_{A^{(e)}} \mathbf{q} \, dA = \iint_{A^{(e)}} \hat{\mathbf{L}}\mathbf{m} \, dA = \int_{\Gamma^{(e)}} \mathbf{T}^T \mathbf{m} \, d\Gamma \quad (55)$$

Choosing now a constant interpolation for the shear forces within each element as  $\mathbf{q} = \mathbf{I}_2 \hat{\mathbf{q}}^{(e)}$ , gives:

$$\hat{\mathbf{q}}^{(e)} = \frac{1}{A^{(e)}} \int_{\Gamma^{(e)}} \mathbf{T}^T \mathbf{m} \, dA \quad (56)$$

Equation (56) requires the evaluation of the bending moments along the element sides. This can be done for the discontinuous bending field case by simple averaging of the corresponding bending moment values contributed by the two adjacent elements sharing each side.

Obviously, the case of a continuous bending field poses no difficulty and (56) can be directly applied to give the shear forces within each element.

## EXAMPLES

The efficiency of the BPT element presented is assessed through different examples of application.

*Simply supported square plate under uniform and point loads*

The geometry of the plate is shown in *Figure 8* where some of the meshes used for the analysis are shown.

A quarter of the plate has been discretized only for symmetry reasons. Note that only structured meshes have been used in this case with the two orientations shown in *Figure 8*.

Numerical results for the central deflection, the central bending moment  $M_x = M_y$ , and the corner vertical reaction for the uniform load case are shown in *Table 2* for meshes of  $5 \times 5$ ,  $10 \times 10$ ,  $20 \times 20$ , and  $30 \times 30$  BPT elements in a quarter of plate (for symmetry reasons) and the two different mesh orientations shown in *Figure 8*. Good convergence to the theoretical exact values<sup>11</sup> is obtained in all cases.

*Figure 9* shows the convergence plots for the central deflection, the central bending moment and the corner reaction *versus* the number of degrees of freedom involved in each solution. Numerical results obtained by Batoz *et al.*<sup>14</sup> using the standard DKT element are also shown for comparison.

The results for the point load case are shown in *Table 3* where the convergence of the central deflection and the corner reaction values is shown again for the two mesh orientations considered. Good results are also obtained in this case with the BPT element.

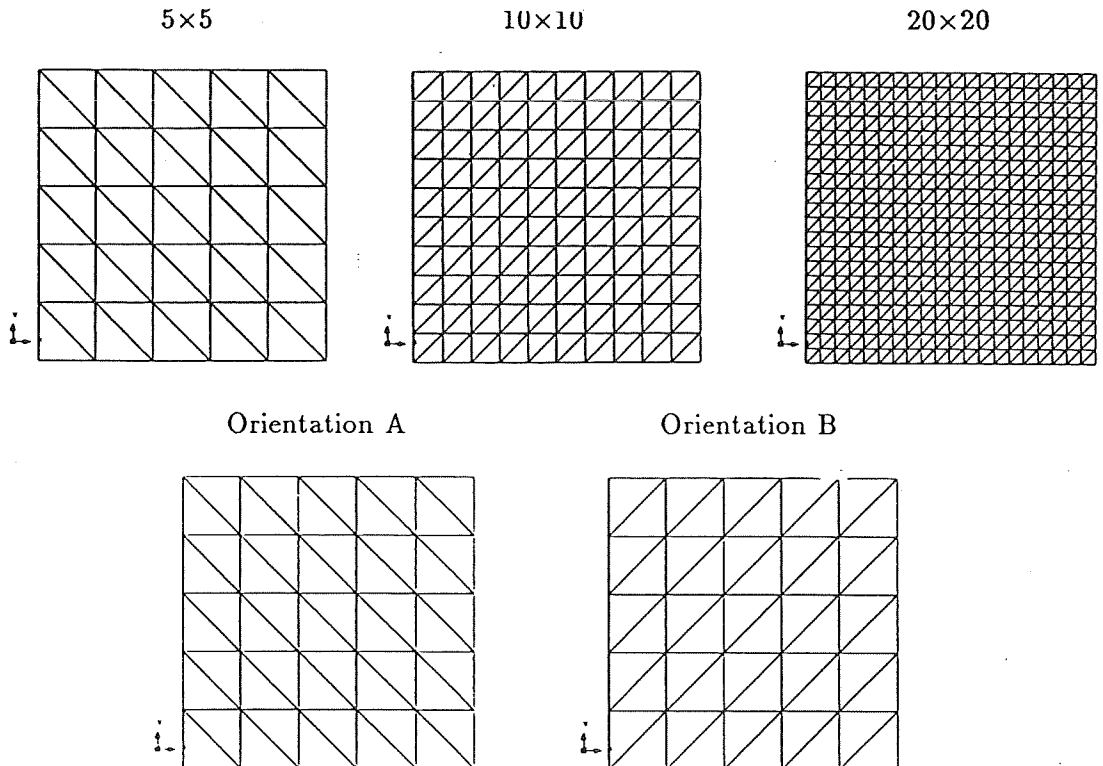


*Figure 8* Square plate. Different meshes used in a quarter of plate for symmetry. Mesh orientations A and B

Table 2 Simple supported square plate under uniform loading. Numerical results obtained using the 3 DOF triangle with meshes of two different orientations A and B (Figure 8)

Mesh	Central deflection ( $\times 10^{-2}$ )		Central moment		Corner reaction	
	A	B	A	B	A	B
5 × 5	0.7925	0.8076	5.4773	5.5416	6.7674	6.5969
10 × 10	0.8272	0.8307	5.7614	5.7651	7.4118	7.0948
20 × 20	0.8462	0.8470	5.8773	5.8756	7.7443	7.4369
30 × 30	0.8527	0.8531	5.9138	5.9095	7.8615	7.5634
Exact <sup>11</sup>	0.8664	0.8664	5.9875	5.9875	8.125	8.125

$$E = 2.0 \times 10^6; \nu = 0.3; t = 0.2; a = 5.0; q = 5.0$$

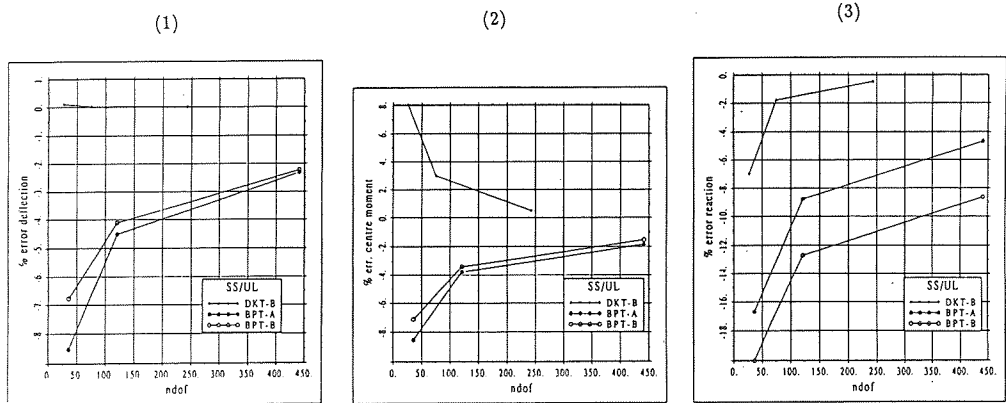


Figure 9 Simple supported square plate under uniform loading. Convergence plots for the central deflection (1), central bending moment (2) and corner reaction (3), for mesh orientations A and B of Figure 8

Table 3 Simple supported square plate under central point load. Numerical results obtained using the 3 DOF triangle with meshes of two different orientations A and B (Figure 8)

Mesh	Central deflection ( $\times 10^{-2}$ )		Corner reaction	
	A	B	A	B
5 × 5	0.1969	0.2012	1.0841	1.0136
10 × 10	0.1947	0.1961	1.1391	1.0852
20 × 20	0.1955	0.1959	1.1744	1.1281
30 × 30	0.1961	0.1963	1.1880	1.1435
Exact <sup>11</sup>	0.1979	0.1979	1.219	1.219

$$E = 2.0 \times 10^6; \nu = 0.3; t = 0.2; a = 5.0; P = 10.0$$

Figure 10 shows the convergence plots for the central deflection and the corner reaction. The results compare well with those obtained by Batoz *et al.*<sup>14</sup> using the DKT element also shown in the same Figure.

Clamped square plate under uniform and point loads

The second example corresponds to the analysis of the same plate of the previous example with clamped edges.

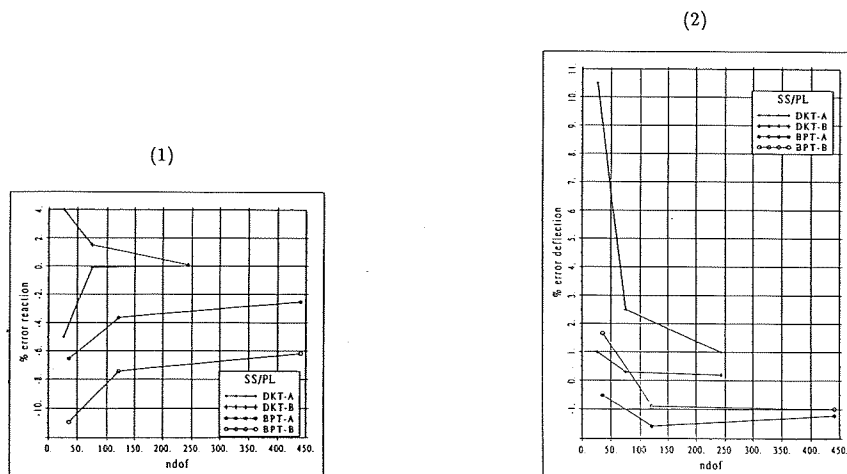


Figure 10 Simple supported square plate under central point load. Convergence plots of central deflection (1) and corner reaction (2) for the two mesh orientations A and B shown in Figure 8

Table 4 Clamped square plate under uniform load. Numerical results obtained using the 3 DOF triangle with meshes of two different orientations A and B (Figure 8)

Mesh	Central deflection ( $\times 10^{-2}$ )		Central moment		Corner reaction	
	A	B	A	B	A	B
5 $\times$ 5	0.2965	0.3099	2.8097	2.9665	-5.8427	-6.2811
10 $\times$ 10	0.2765	0.2794	2.8550	2.8900	-6.1985	-6.4349
20 $\times$ 20	0.2715	0.2722	2.8614	2.8700	-6.3224	-6.4472
30 $\times$ 30	0.2705	0.2709	2.8624	2.8663	-6.3561	-6.4427
Exact <sup>11</sup>	0.2698	0.2698	2.8875	2.8875	-6.4125	-6.4125

$$E = 2.0 \times 10^6; \nu = 0.3; t = 0.2; a = 5.0; q = 5.0$$

Numerical results for the central deflection, the central bending moment and the mid-side moment under uniform load for different meshes are shown in Table 4.

The convergence plots of these values is shown in Figure 11 for the purpose of comparison with the DKT results for the same problem<sup>14</sup>.

Table 5 shows the results for the central deflection and the mid-side moment for different meshes. The same values are plotted in Figure 12 where results obtained using the DKT element are also shown<sup>14</sup>. Convergence plots shown in Figure 12 indicate that the 3 DOF plate triangle proposed is less sensitive to mesh orientation than the DKT element.

#### Circular plates under uniform loading

The geometry of the circular plate is shown in Figure 13 together with the different meshes used.

Numerical results obtained for the simply supported and clamped cases are shown in Tables 6a and 6b.

Excellent results are obtained with relatively coarse meshes for both the central deflections and the central bending moments as it can be seen in these Tables.



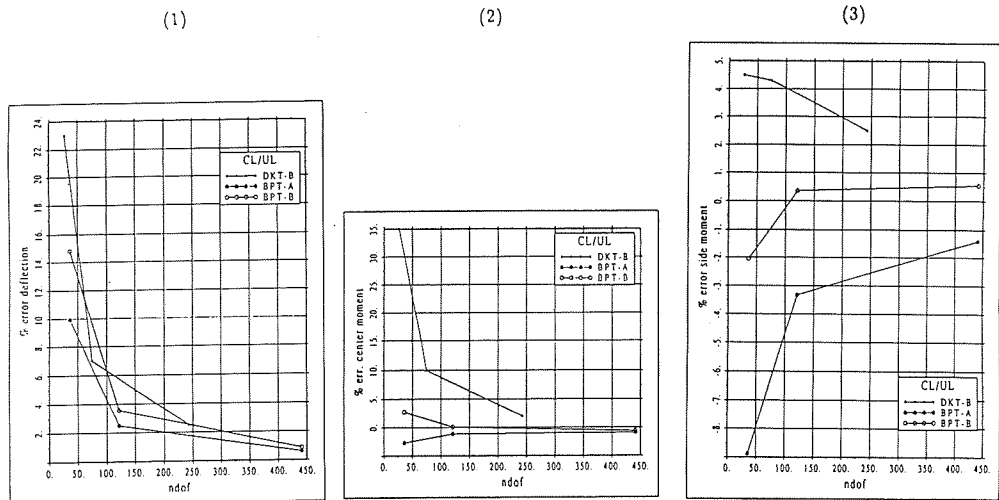


Figure 11 Clamped square plate under uniform loading. Convergence plots for the central deflection (1), the central bending moment (2) and the mid-side bending moment (3) for the two mesh orientations A and B shown in Figure 8

Table 5 Clamped square plate under point load. Numerical results obtained using the 3 DOF triangle with meshes of two different orientations A and B (Figure 8)

Mesh	Central deflection ( $\times 10^{-3}$ )		Mid-side moment	
	A	B	A	B
5 × 5	1.091	1.149	-1.1323	-1.2036
10 × 10	0.9971	0.1014	-1.2112	-1.2523
20 × 20	0.9689	0.9739	-1.2406	-1.2603
30 × 30	0.9629	0.9654	-1.2475	-1.2607
Exact <sup>11</sup>	0.9555	0.9555	-1.257	-1.257

$$E = 2.0 + 10^6; \nu = 0.3; t = 0.2; a = 5.0; q = 5.0; P = 10$$

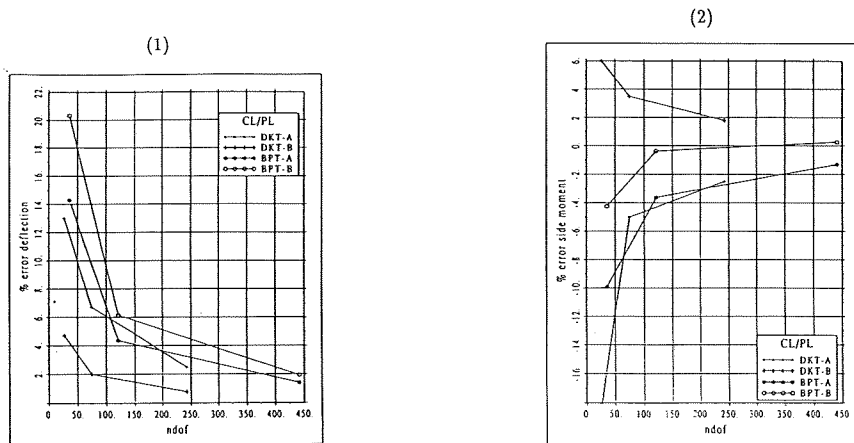


Figure 12 Clamped square plate under point loading. Convergence plots of central deflection (1) and mid-side bending moment (2) for the two mesh orientations A and B shown in Figure 8

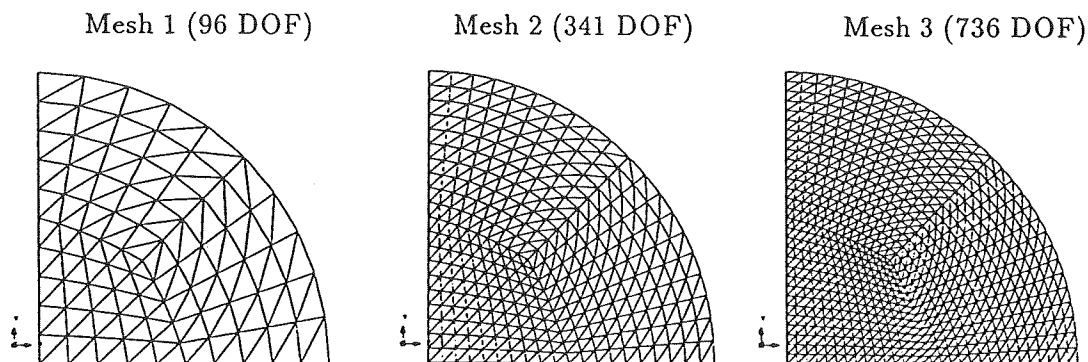


Figure 13 Circular plate. Different meshes used in a quarter of plate for symmetry

Table 6 Circular plate under uniform loading. Results for simple supported (a) and clamped (b) plate

Mesh	DOF	$w_0$	$M_r^0$	$M_t^0$
1	96	39105.4	5.0186	5.0186
2	341	39518.2	5.1075	5.1075
3	736	39611.5	5.1275	5.1275
Exact <sup>11</sup>		39813.7	5.1562	5.1562

(b)

Mesh	DOF	$w_0$	$M_r^0$	$M_t^0$
1	96	9914.84	1.9820	1.9820
2	341	9790.91	2.0147	2.0147
3	736	9768.17	2.0219	2.0219
Exact <sup>11</sup>		9765.62	2.0312	2.0312

$$E = 10.92; \nu = 0.3; t = 0.1; R = 5.0; q = 1.0$$

### CONCLUDING REMARKS

A general methodology for deriving thin plate elements with only a translational degree of freedom has been presented. The methodology can be applied to derive new single nodal degree of freedom plate elements of triangular and quadrilateral shapes with different approximations. The efficiency of the simple 3 DOF triangle proposed has been shown with different examples of applications. This element (termed BPT) has a promising future for more complex plate and shell problems involving dynamics, non-linear effects and mesh adaptivity.

One of the key issues of the proposed approach lays in the evaluation of the deflection gradient along the element sides. Indeed other more accurate techniques than the simple derivative averaging procedure used in this paper could be used to enhance the element approximation. Among these special finite difference energy techniques<sup>15</sup>, derivative recovery procedures<sup>16</sup> or diffuse element methods<sup>17</sup> could be effectively combined with the approach proposed in this paper for enhanced derivative computation leading to improvements in the BPT element performance.

## ACKNOWLEDGEMENTS

The authors are grateful to Prof. O. C. Zienkiewicz for many useful comments during the development of this work.

## REFERENCES

- 1 Uguraz, A. C. *Stresses in Plates and Shells*, McGraw-Hill, New York (1981)
- 2 Barnes, M.R. Form finding and analysis of tension space structure by dynamic relaxation, *PhD Thesis*, Dept. of Civil Engineering, The City University, London (1977)
- 3 Hampshire, J. K., Topping, B. H. V. and Chan, H. C. Three node triangular elements with one degree of freedom per node, *Eng. Comput.*, **9**, 49–62 (1992)
- 4 Phaal, R. and Calladine, C. R. A simple class of finite elements for plate and shell problems. I: Elements for beams and thin plates, *Int. J. Num. Meth. Eng.*, **35**, 955–977 (1992)
- 5 Phaal, R. and Calladine, C. R. A simple class of finite elements for plate and shell problems. II: An element for thin shells with only translational degrees of freedom, *Int. J. Num. Meth. Eng.*, **35**, 979–996 (1992)
- 6 Patankar, S. V. *Numerical Heat Transfer and Fluid Flow*, Series in Computational Methods in Mechanics and Thermal Sources (Eds. W. J. Minkowycz and E. M. Sparrow), Hemisphere, New York (1980)
- 7 Hirsch, C. *Numerical Computations of Internal and External Flow*, Vol. I, John Wiley, New York (1989)
- 8 Zienkiewicz, O. C. and Oñate, E. Finite elements versus finite volumes. Is there really a choice?, *Non Linear Computational Mechanics. State of the Art* (Eds. P. Wriggers and R. Wagner), Springer Verlag, Heidelberg (1991)
- 9 Oñate, E., Cervera, M. and Zienkiewicz, O. C. A study of the finite volume method for structural mechanics, *Res. Rep.*, **15**, CIMNE, Barcelona (1992); submitted to *Int. J. Num. Meth. Eng.*
- 10 Idelsohn, S. and Oñate, E. Finite elements and finite volumes for CFD. Two good friends, *Res. Rep.*, **15**, CIMNE, Barcelona (1992); *Int. J. Num. Meth. Eng.* in press
- 11 Timoshenko, S. *Theory of Plates and Shells*, McGraw-Hill, New York (1979)
- 12 Zienkiewicz, O. C. and Taylor, R. L. *The Finite Method Element Method*, 4th Edn, McGraw-Hill, New York, Vol. I (1990) and Vol. II (1991)
- 13 Oñate, E. *The Finite Element Method for Structural Analysis*, CIMNE, Barcelona (1993)
- 14 Batoz, J. L., Bathe, K. J. and Ho, L. W. A study of three-node triangular plate bending elements, *Int. J. Num. Meth. Eng.*, **28**, 533–560 (1989)
- 15 Pavlin, V. and Perrone, N. Finite difference energy techniques for arbitrary meshes applied to linear plate problems, *Int. J. Num. Meth. Eng.*, **14**, 647–669 (1979)
- 16 Zienkiewicz, O. C. and Zhu, J. Z. Superconvergence derivative recovery techniques and a posteriori error estimator in the FEM, Part I: General superconvergent recovery technique, and Part II, *Int. J. Num. Meth. Eng.* **33**, 1331–1382 (1992)
- 17 Nayroles, B., Rouzot, G. and Villon, P. Generalizing the finite element method—diffuse approximation and diffuse elements, *Comput. Mech.*, **10**, 307–318 (1992)
- 18 Oñate, E. and Cervera, M. A general procedure for deriving thin plate bending elements with one degree of freedom per node, *Res. Rep.* **32**, CIMNE, Barcelona (1993)
- 19 Brunet, M. and Sabourin, F. A simplified triangular shell element with necking criterion for 3D sheet forming analysis, in *NUMISHEET 93* (Eds Makinouchi, A., Nakamachi, E., Oñate, E. and Wagoner, R. H.), RIKEN, Tokyo (1993)

